

Leidenfrost temperature increase for impacting droplets on carbon-nanofiber surfaces

Hrudya Nair,^{†,‡,¶,||} Hendrik J. J. Staat,^{†,||} Tuan Tran,^{*,†,⊥} Arie van Houselt,^{‡,¶}
Andrea Prosperetti,^{†,§} Detlef Lohse,^{*,†,¶} and Chao Sun^{*,†,¶}

Physics of Fluids, University of Twente, P. O. Box 217, 7500 AE Enschede, The Netherlands, Catalytic Processes and Materials, University of Twente, P. O. Box 217, 7500 AE Enschede, The Netherlands, MESA+ Institute for Nanotechnology, University of Twente, P. O. Box 217, 7500 AE Enschede, The Netherlands, and Department of Mechanical Engineering, Johns Hopkins University, Baltimore, MD 21218, USA

E-mail: tran@ntu.edu.sg; d.lohse@utwente.nl; c.sun@utwente.nl

Abstract

Droplets impacting on a superheated surface can either exhibit a contact boiling regime, in which they make direct contact with the surface and boil violently, or a film boiling regime, in which they remain separated from the surface by their own vapor. The transition from the contact to the film boiling regime depends not only on the temperature of the surface and kinetic energy of the droplet, but also on the size of the structures fabricated on the surface. Here we experimentally show that surfaces covered with carbon-nanofibers delay the transition to film boiling to much higher temperature compared to smooth surfaces. We present physical arguments showing that, because of the small scale of the carbon fibers, they are cooled by the vapor flow just before the liquid impact, thus permitting contact boiling up to much higher temperatures than on smooth surfaces. We also show that, as long as the impact is in

the film boiling regime, the spreading factor of impacting droplets follows the same $We^{3/10}$ scaling (with We the Weber number) found for smooth surfaces, which is caused by the vapor flow underneath the droplet.

Introduction

Spray cooling is an effective heat transfer mechanism as it is capable of delivering spatially uniform and high heat transfer rates (see e.g.¹⁻³). An important new application of this technology is in electronic cooling, where the growing power consumption and decreasing sizes pose increasingly challenging heat dissipation demands (see e.g.^{4,5}). Other common situations in which cold drops impact hot surfaces are found in internal combustion engines (see e.g.^{6,7}), quenching of aluminum and steel (see e.g.⁸), fire suppression (see e.g.^{9,10}) and others.

In all these applications a stream of fine droplets dispensed, e.g., from a nozzle impinges on a solid surface and cools it by a combination of sensible heat absorption and latent heat of vaporization. Due to the inherent complexity of the phenomenon and the large number of parameters involved, such as droplet size, velocity distribution, droplet number density and material properties, many aspects of the physical mechanisms involved still remain incompletely understood.^{1,11,12}

*To whom correspondence should be addressed

[†]Physics of Fluids, University of Twente, P. O. Box 217, 7500 AE Enschede, The Netherlands

[‡]Catalytic Processes and Materials, University of Twente, P. O. Box 217, 7500 AE Enschede, The Netherlands

[¶]MESA+ Institute for Nanotechnology, University of Twente, P. O. Box 217, 7500 AE Enschede, The Netherlands

[§]Department of Mechanical Engineering, Johns Hopkins University, Baltimore, MD 21218, USA

^{||}These authors contributed equally to this work.

[⊥]Present address: School of Mechanical and Aerospace Engineering, Nanyang Technological University, 50 Nanyang Avenue, Singapore 639798

A fundamental understanding of the impact of an individual droplet on superheated surfaces is the first step toward a better understanding and eventual optimization of the process. Various aspects of this particular problem have been investigated, such as the effect of droplet size, velocity, physical properties (see e.g.^{13,14}), and surface roughness (see e.g.^{15,16}), the transition between different boiling regimes (see e.g.^{16–20}), the surface temperature change and heat transfer during impact (see e.g.^{15,21–23}), the residence time of the impacting droplet (see e.g.^{16,24}), the spreading factor (see e.g.^{16,20,25}) and others.

An important quantitative feature of the phenomenon is the transition temperature T_L between the contact boiling regime, where the liquid makes direct contact with the heated surface, and the film boiling regime, where a stable vapor layer between the liquid and the surface is formed during impact. As the rate of heat transfer in the film boiling regime is significantly reduced due to the poor thermal conductivity of the vapor layer, this regime should be avoided for applications that require high heat transfer rates. Methods to increase T_L , or delay the onset of the film boiling regime, are therefore of great interest for such applications.

Recently, surfaces covered with nanofibers were shown to effectively enhance the heat transfer from the surface to a liquid in contact with it.^{23,26} In particular, it was reported that for impacting ethanol droplets on surfaces covered with nanofiber mats, the film boiling behavior was not observed even when the surface temperature was as high as 300°C,²² which implies that the transition temperature to film boiling is *increased* compared to that observed on smooth surfaces. This is in marked contrast with the impact on surfaces covered with *microstructures*, for which the transition temperature is considerably *decreased* compared to a smooth surface.¹⁶ Indeed, numerous questions regarding the effects of nanostructures on the transition temperature are still open. First of all, why do nanofibers cause a higher T_L compared to that on smooth surfaces? And, further, what is the transition temperature T_L on this type of surfaces? how does it change with the size of the nanostructures on the surfaces?

To answer these questions, in this paper we study the impact of droplets on heated surfaces covered

with carbon nanofibers (CNF), which are carbonaceous structures grown by catalytic vapor deposition of hydrocarbons. This type of nanostructures is well-known for their unique physical and chemical properties with a tunable morphology (the diameter can be varied from a few to hundreds of nanometers, the height can be controlled from a few micrometers to millimeters), which in turn can be exploited for tuning the roughness, porosity, and surface area.²⁷

We use two types of CNF surfaces corresponding to two different typical fiber lengths and a smooth silicon surface. For each type of surface, we determine the transition temperature and its dependence on the impact velocity. We propose a quantitative explanation of the effect of nanofibers on the transition temperature T_L . Furthermore, for impact of droplets in the film boiling regime, we measure the spreading factor and compare our data with existing models.

Experimental details

Synthesis of carbon nanofiber layers

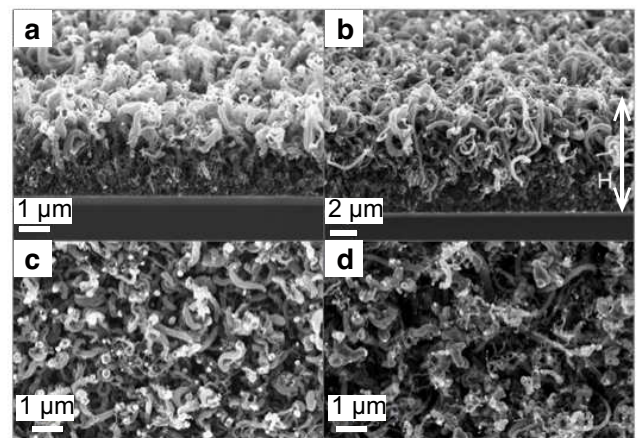


Figure 1: Scanning electron microscope (SEM) images showing side views of the carbon nanofiber (CNF) layers with a synthesis time of (a) 11 min and (b) 14 min. The arrow in (b) indicates the height H of the CNF layer. The corresponding top-view SEM images are shown in (c) for a synthesis time of 11 min and in (d) for a synthesis time of 14 min. The bar represents 1 μm in (a), (c) and (d), and 2 μm in (b).

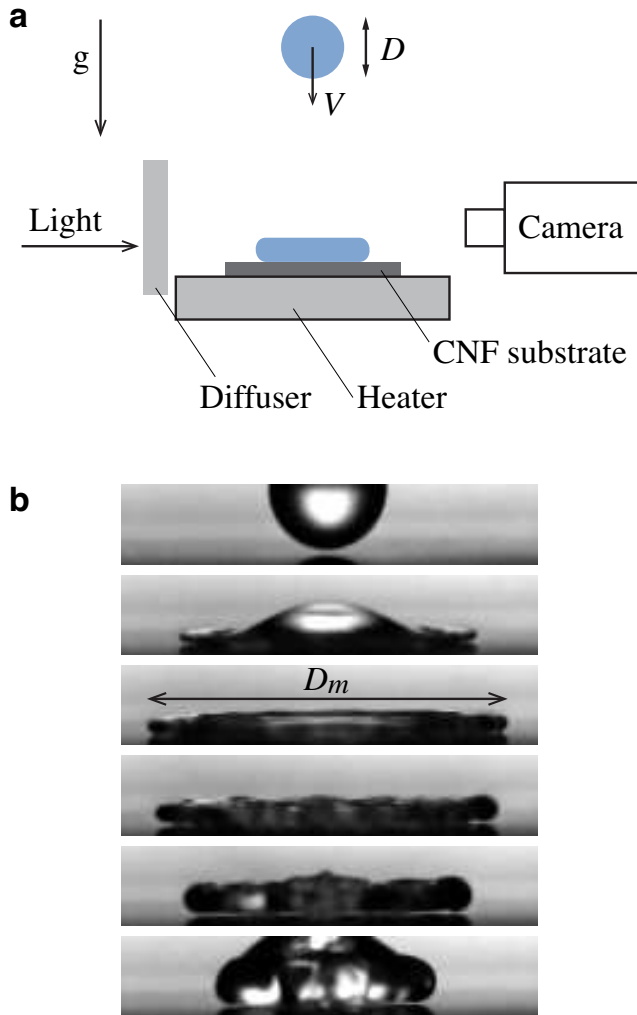


Figure 2: (a) Schematic (not to scale) of the experimental setup used to observe the characteristic behaviors of impacting droplets on heated surfaces. The surface of interest is placed on a heater, which can be heated up to 500°C . FC-72 droplets of diameter D impact the heated sample with impact velocity V . The behavior of the impacting droplets is recorded from the side by a high-speed camera (Photron SA1.1). From the recordings, D , V , and the maximum spreading D_m of the droplet can be measured. (b) Series of snapshots of an impacting droplet in the film boiling regime showing how D_m is measured as the maximum horizontal extension of the droplet.

Carbon nanofibers (CNFs) were synthesized on oxidized silicon wafers (p-type, $5 - 10\text{Ohm-cm}$ resistivity, 100mm diameter, $525 \pm 25\mu\text{m}$ thickness, $\{100\}$ crystal orientation; Okmetic Finland) using nickel (Ni) thin film as catalyst. First, a SiO_2 layer of 220nm thickness was grown via wet oxidation (45min , 1000°C) on these silicon substrates. Second, a pattern was defined in spin-coated photoresist (Olin, 906-12), resulting in unmasked squares of $8\text{mm} \times 8\text{mm}$, by means of standard UV lithography (EVG 620). Further, a 10nm tantalum layer followed by a 25nm nickel layer was deposited via electron-beam evaporation. Finally the samples were subjected to an ultrasonic lift-off step in acetone ($> 20\text{min}$; VLSI 100038, BASF), followed by rinsing in water and spin drying. These nickel-coated substrates were diced into $1\text{cm} \times 1\text{cm}$ samples (Disco DAD-321 dicing machine). To remove organic contaminants, these samples were ultrasonically cleaned in acetone (10min , Branson 200 ultrasonic cleaner) and de-ionized water (2min , 25°C).²⁸

After drying with synthetic air, the samples were placed centrally on a flat quartz boat inside a quartz reactor and were loaded into a horizontal oven equipped with three temperature controllers along it. Nitrogen (N_2 ; 99.999%, INDUGAS NV.) was used as carrier gas during heating, pretreatment, CNF synthesis and cooling. First, the temperature was increased (5Kmin^{-1}) to 500°C . Second, the samples were pretreated with 20 vol.% of hydrogen (H_2 ; 99.999%, INDUGAS NV.) for 2 hours at a total flow rate of 50mlmin^{-1} in order to reduce the passivated Ni thin film. Subsequently the temperature was increased (5Kmin^{-1}) to 635°C , at which temperature the CNF synthesis was performed via catalytic vapor decomposition using 25 vol.% ethylene (C_2H_4 ; 99.95% Praxair Inc.) and 6.25 vol.% H_2 in a total flow rate 100mlmin^{-1} . Finally the samples were cooled down to room temperature (10Kmin^{-1}).

Two sets of samples were used for the droplet impact studies. One set was obtained after a CNF synthesis time of 11min , resulting in a CNF layer thickness $3.4 \pm 0.3\mu\text{m}$. The other set was obtained after a CNF synthesis time of 14min , resulting in a CNF layer thickness of $7.5 \pm 0.7\mu\text{m}$. More details of the influence of synthesis time on CNF layer thickness have been reported previously.²⁸

These samples will be termed as CNF(3.5) and CNF(7.5), respectively. 1 shows representative scanning electron microscope (SEM) images with the side views (1(a) and (b)) and top views (1(c) and (d)) of the surfaces CNF(3.5) and CNF(7.5).

The thickness of the CNF layers was determined using 5 representative cross-sectional SEM images taken at various positions on the sample (10 height measurements were averaged per SEM image). The width of the nanofibers ranges from 32 nm to 220 nm with average value of 127 nm.

Experimental method

A schematic diagram of the experimental setup is shown in 2. All droplet impact experiments were performed with FC-72 (3M Fluorinert Electronic Liquid), a dielectric fluid commonly used in electronics cooling applications. The liquid has boiling point $T_b = 56^\circ\text{C}$, density $\rho_l = 1680\text{kgm}^{-3}$, and surface tension $\sigma = 0.01\text{Nm}^{-1}$. We generate droplets by using a syringe pump (PHD 2000 Infusion, Harvard Apparatus) to inject liquid into a small fused silica needle where the droplets are formed at the tip. The flow rate is kept at a small value ($\approx 0.1\text{mLmin}^{-1}$) so that droplet detachment from the needle is due only to gravitational force, hence keeping the droplet size uniform. After detaching from the needle, a droplet falls on the target surface placed on a brass plate with a cartridge heater and a thermocouple (Omega Inc.) embedded inside. The surface temperature T was set by a controller and was varied between 60°C and 450°C . This temperature was also measured independently by a surface temperature probe (Tempcontrol B.V.). The difference between the controller's set point and the surface probe measurement was less than 3K. Thus we take the controller's set point as the surface temperature T of the surface.

Recordings of the impact events were made with a high-speed camera (Photron SA1.1) (see 2). From these high-speed recordings, the boiling behaviors were analyzed, and the droplet diameter D , the impact velocity V and the maximum spreading diameter D_m (see 2) were measured. From the measured diameter and velocity, we calculated the Weber number $We = \rho_l DV^2 / \sigma$, which is a dimensionless number that characterizes the droplet's ki-

netic energy compared to its surface energy. The impact velocity V was varied by changing the needle's height. Impact events were repeated at least three times for every combination of V and T to test reproducibility of the experiment.

Characterization of boiling behavior

By varying the surface temperature between 60°C and 450°C and the Weber number between 10 and 1000, we observed two characteristic boiling behaviors: contact boiling and film boiling. In 3 we show two series of images to illustrate the difference between these two regimes. The essential difference between the two is whether or not the liquid makes direct contact with the heated surface during impact.^{20,29,30} In the contact boiling regime (3(a)), as the pressure of the vapor generated underneath the droplet is not sufficient to support the droplet's dynamic pressure, the liquid touches the heated surface and quickly boils due to the high heat flux through the contact area. The recorded snapshots show the small droplets ejected as a result of the boiling process. In contrast, an impacting droplet in the film boiling regime is separated from the heated surface by a developing vapor layer (see 3(b)). This vapor layer insulates the droplet during the impact time, hence prevents the liquid from boiling violently.

By carefully analyzing the recorded movies of impacting droplets, we categorized the impact as being in the film boiling regime when droplet ejection or vapor bubble generation were not observed.

Results and discussions

Dynamic Leidenfrost temperature

In 4 we show phase diagrams of the characteristic boiling behavior of impacting droplets on smooth silicon surfaces, CNF(3.5), and CNF(7.5), respectively. The temperature ranges were 60°C to 250°C for the smooth silicon surfaces, 60°C to 300°C for the CNF(3.5) surfaces, and 100°C to 450°C for the CNF(7.5) surfaces. In each phase diagram, there is a clear transition between the contact and the film boiling regimes. This transition temperature is marked by a solid line, with

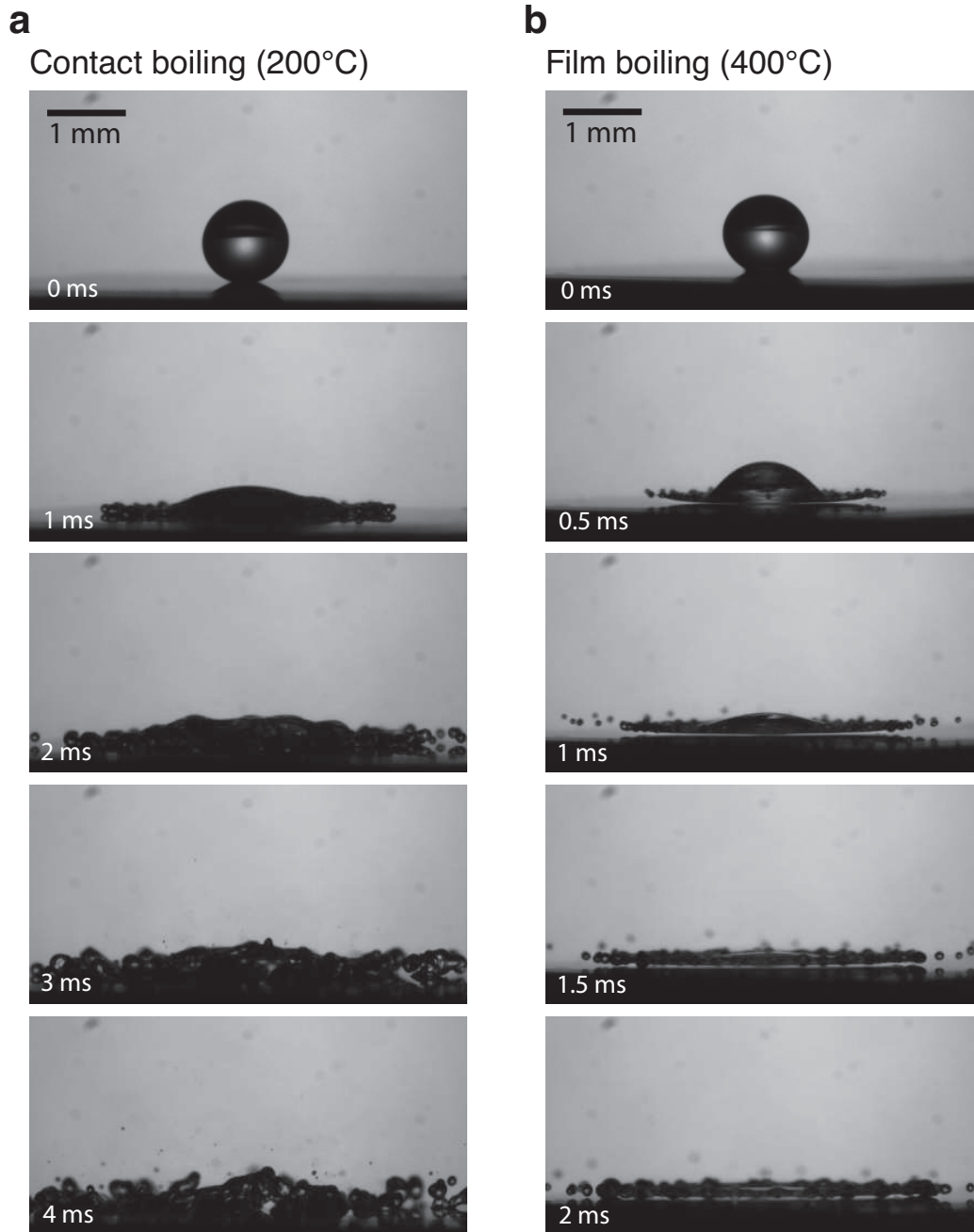


Figure 3: (a) Representative images showing the characteristic boiling behavior of an impacting FC-72 droplet on a 7.5 μm -thick CNF surface in the contact boiling regime, $T = 200^\circ\text{C}$. The diameter of the impacting droplet is $D = 1.1\text{ mm}$, the impact velocity $V = 1.0\text{ m/s}$ and the Weber number $We = 154$. (b) Representative images of a FC-72 droplet with the same diameter and velocity impacting on the same surface as in (a), but at the higher surface temperature, $T = 400^\circ\text{C}$. In this case, the impact is in the film boiling regime.

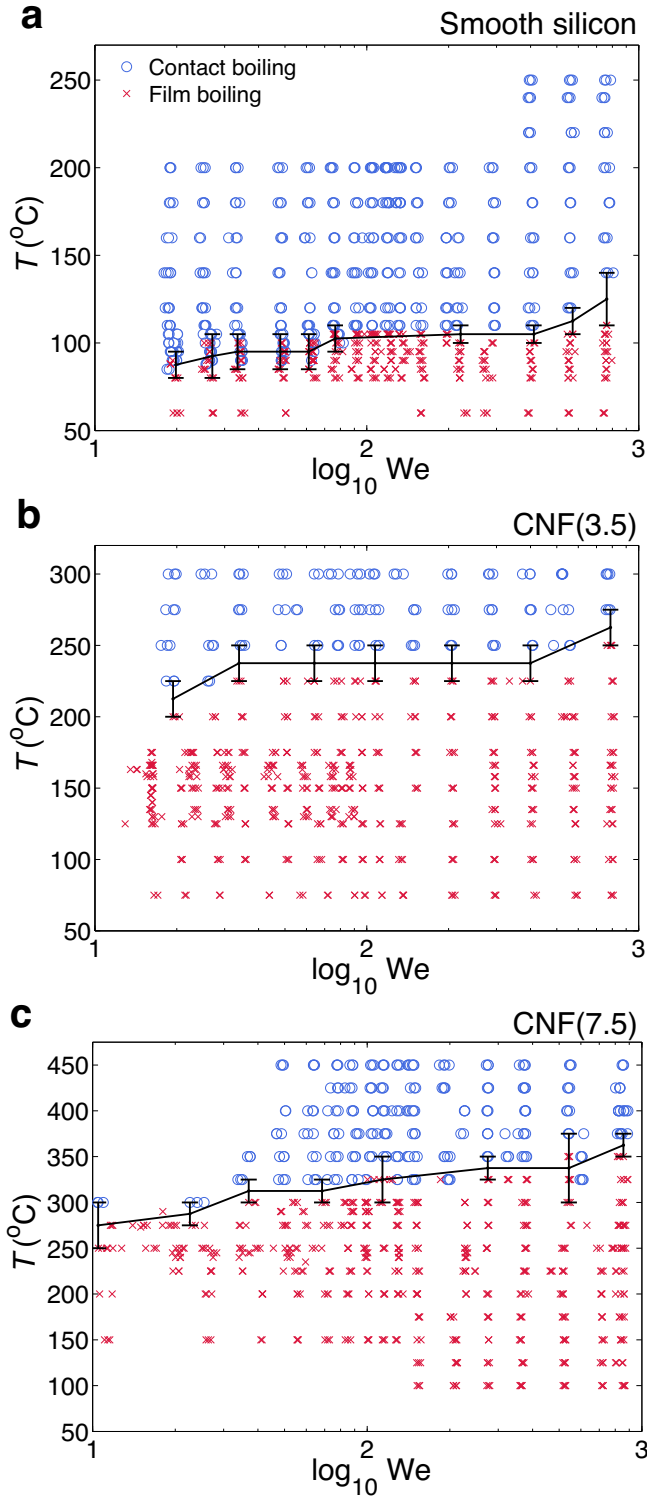


Figure 4: (a) Phase diagram showing the characteristic boiling behaviors of impacting FC-72 droplets on smooth silicon surfaces. The contact boiling regime (red crosses) and film boiling regime (open blue circles) are separated by a transition band, indicated by the vertical bars, where both characteristic behaviors were observed. (b) Phase diagram for surfaces covered by a 3.5 μm -thick CNF layer. (c) Phase diagram for surfaces covered by a 7.5 μm -thick CNF layer. Note the much larger temperature ranges in (b) and (c).

the vertical bars indicating the intermediate region where both boiling behaviors were observed. The transition temperature, known as the dynamic Leidenfrost temperature T_L , increases with increasing kinetic energy of impacting droplets. This dependence of T_L on We is qualitatively similar to that found previously for droplets impacting on smooth and micro-structured surfaces,^{15,16,20} and is expected: the increasing momentum of the impact forces the droplet into contact with the surface at larger and larger temperature.

These results, however, are in stark contrast with those found for smooth and microstructured surfaces in two respects, as can be seen from 5 in which T_L for the smooth and CNF surfaces is compared. The first unexpected finding is that, while T_L is lower for microstructured surfaces as compared with smooth ones,¹⁶ it is actually higher in the case of carbon nanofibers. For example, for $We = 100$, T_L for the smooth surface is 110 °C, whereas for CNF(3.5) and CNF(7.5) it increases to 250 °C and 350 °C, respectively. Secondly, T_L increases with nanofiber length, again in contrast with surfaces covered with micrometer-size pillars for which, for given shape and spacing, the microstructure height is inversely correlated with T_L .¹⁶ The tentative explanation of that latter finding offered in Ref.¹⁶ is that the surface of the impacting liquid tends to penetrate the space between the pillars. This causes the liquid surface area to increase, the more the higher the pillars. As a consequence, the vapor generation rate also increases and the film boiling regime sets in at a lower temperature.

As explanation of the opposite behavior found with carbon nanofibers we suggest that they are efficiently cooled by the vapor flow before the drop touches the CNF surface. To support this conjecture in the following subsection we will estimate the time scale τ_c for the temperature of the nanofibers to cool, and compare it with the time scale τ_e the nanofiber is exposed to the vapor flow (which will be found to be somewhat larger), and also with the time scale τ_h for the heat flow inside the nanofiber (which will be found to be much larger).

Estimate of the relevant time scales

We start with the estimate for the time scale τ_c for the cooling of the nanofibers by the “vapor wind”. Since the cross section of the nanofibers is of the order of 100 nm, the time scale τ_c can be estimated by assuming their temperature to be uniform, which is the so-called lumped capacitance approximation (see e.g.³¹). This time scale can then be estimated to be

$$\tau_c \sim \frac{w\rho_n C_n}{h}, \quad (1)$$

in which w is the diameter of the nanofiber, ρ_n and C_n its density and specific heat, and h the heat transfer coefficient. The latter can be expressed in terms of a Nusselt number, $\text{Nu} = wh/K_v$, with K_v the vapor thermal conductivity, so that

$$\tau_c = \frac{\rho_n C_n w^2}{K_v \text{Nu}} = \frac{\rho_n C_n}{\rho_v C_v} \frac{w^2}{\kappa_v \text{Nu}}, \quad (2)$$

in which ρ_v , C_v , and κ_v are the vapor density, specific heat, and thermal diffusivity, respectively. The (approximate) proportionality of τ_c to the square of the fiber size is a particularly noteworthy feature of this expression. In standard correlations (see e.g.³¹), Nu is given as a function of the fluid Prandtl and Reynolds numbers. No measured value for the former seems to be available for FC-72 vapor, but it is well known that the Prandtl number of gases is close to 1 and we can safely use this estimate here. Estimation of the Reynolds number requires a value for the viscosity of the vapor which, again, does not seem to have been measured. The order of magnitude of the viscosity of many gases and vapors is 10^{-5} Pa s, and this is the value we will use. The density of FC-72 vapor at the boiling point 56 °C is about 11.5 kg/m³. Taking $w \sim 100$ nm and using these values we then find $\text{Re} \sim 0.1 V_v$, with V_v the vapor velocity in m/s. This quantity has been estimated in¹⁶ (see equation (13) of that paper) where it was found to be of the order of

$$V_v \sim \left(\frac{\rho_l C_v \Delta T}{\rho_v L \text{Pr}_v} \right)^{1/2} V, \quad (3)$$

with ρ_l the liquid density, ΔT the liquid-surface temperature difference, L the latent heat and Pr_v

the vapor Prandtl number. With $\rho_l = 1680$ kg/m³, $L = 88$ kJ/kg, $C_v = 910$ J/kg K and $\rho_v = 11.5$ kg/m³ (values at 56 °C), $\Delta T \sim 100$ K, V the impact velocity ~ 1 m/s and again taking $\text{Pr}_v \sim 1$, we find $V_v \sim 12$ m/s so that $\text{Re} \sim 1.2$. The Churchill-Bernstein correlation³¹ then gives a Nusselt number of about 1. Use of equation (??) requires values of K_v or κ_v , neither of which seems to be available. For many gases and vapors κ_v is of the order of 10^{-5} m²/s. With this estimate, taking $\rho_n \simeq 2267$ kg/m³, $C_n \simeq 709$ J/kg K and, again, $w \sim 100$ nm, we find from eq. (??) $\tau_c \simeq 150$ ns.

This time scale has to be compared with the characteristic time τ_e during which the fiber is exposed to the cooler vapor until the liquid makes contact with it, which can be estimated as

$$\tau_e \sim \frac{H_v}{V}, \quad (4)$$

where $H_v \sim D \text{St}^{-2/3}$ is the characteristic thickness of the vapor layer at which the drop starts being deformed due to the increasing pressure on its underside.³² Here, as above, D is the droplet diameter, V is the impact velocity, and $\text{St} = \rho_l V D / \mu_v$ is the Stokes number, where μ_v is the viscosity of vapor. Hence we obtain the time during which the nanofibers are exposed to the cooler vapor flow $\tau_e \sim D \text{St}^{-2/3} / V$. In the use of this estimate we again encounter the problem that μ_v is not available but, if we use the same estimate $\mu_v \sim 10^{-5}$ Pas as before and take $V \simeq 1$ m/s, $D \simeq 1$ mm, we find $\tau_e \simeq 330$ ns, which is seen to be long enough to cause a substantial cooling of the fibers.

Of course, as the fibers are cooled by the vapor, heat flows towards their tips from the silicon substrate with a characteristic time

$$\tau_h = \frac{\ell^2}{\kappa_c}, \quad (5)$$

in which ℓ is the fiber length and κ_c its thermal diffusivity of the carbon nanofibers. Since, in this experiment, the fibers had not been heat-treated, we can estimate their thermal conductivity on the basis of the results of Ref.³³ as $K_c = 4.6$ W/m K and, therefore, $\kappa_c \sim 2.86 \times 10^{-6}$ m²/s. For the shorter fibers $\ell \simeq 3.4$ μm and, therefore, $\tau_h \sim 4$ μs while, for the longer fibers, $\ell \simeq 7.5$ μm and $\tau_h \sim 20$ μs . These times are much longer than both the cool-

ing time and the exposure time to the vapor flow, which implies that the liquid encounters fibers at a much cooler temperature than the core silicon substrate. This circumstance would explain why the CNF surfaces require a higher temperature to achieve the film boiling regime compared to the smooth surfaces, and why the transition temperature increases with the fiber length.

The size of the cross section of the fibers in our experiment is close to the cross-over value at which cooling and exposure to the vapor flow have comparable time scales. It follows that fibers or, more generally, microstructures with a larger cross section would be insensitive to the cooling effect. As a check of this expectation we can apply the same estimates to the case of the microstructured surfaces studied earlier.¹⁶ In that case the fluid was water for which, of course, all the required physical properties are well known. The microstructures had the form of silicon pillars with a square cross section of about $10 \times 10 \mu\text{m}^2$ and heights from 2 to 8 μm . The vapor velocity estimated from eq. (??), again with $\Delta T \sim 100\text{K}$ and $V \sim 1 \text{ m/s}$, is found to be $V_v \sim 12 \text{ m/s}$. The corresponding Reynolds number is $\text{Re} \sim 6$ with a corresponding Nusselt number $\text{Nu} \sim 1.7$. In this case $\rho_n = 2330 \text{ kg/m}^3$, $C_n = 705 \text{ J/kg K}$ and eq. (??) gives $\tau_c \sim 6.6 \text{ ms}$. The exposure time to the vapor is not very different from the previous estimate, and is therefore several orders of magnitude shorter. It is evident that, in this case, the vapor flow is just a small perturbation which does not have an appreciable effect on the pillar temperature.

Spreading factor

We devote this section to quantifying the spreading factor of impacting droplets in the film boiling regime. The spreading factor is defined as D_m/D , where D_m is the maximum spreading diameter. In fig. 6, we show a log-log plot of D_m/D versus We for all the impact experiments obtained on smooth and CNF surfaces. All the data points were collected for impacts in the film boiling regime and in the course of which the droplets did not disintegrate during the expanding phase. The Weber number ranges from 5 to 600. All data sets collected from the three different surfaces collapse on the same curve, show-

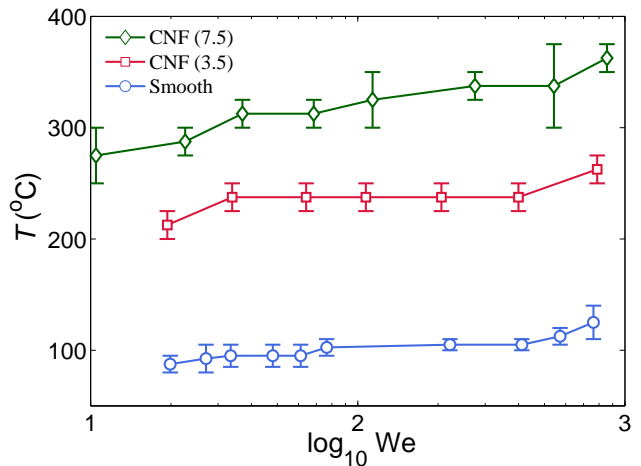


Figure 5: Dynamic Leidenfrost temperature (transition from contact to film boiling) for smooth silicon, and surfaces covered by a 3.5 μm - and a 7.5 μm -thick layer of carbon nanofibers.

ing that the spreading dynamics does not depend on the features and temperature of the surfaces. This result is consistent with the recent study of impacting droplets on micro-structured surfaces,¹⁶ which showed that the spreading factor is independent of the microstructures and depends very weakly on the surface temperature. Moreover, the spreading factor is in agreement with the scaling $D_m/D \propto We^{3/10}$. This scaling law embodies the main assumption that the spreading of the liquid is driven by the vapor flow underneath the droplet.¹⁶ As a result, we conclude that the presence of the carbon nanofibers only changes the transition temperature to film boiling of the impacting droplets, but does not affect the dynamics of the vapor flow in the film boiling regime or the liquid spreading.

Conclusions

We have explored the phase space (We, T) of impact of FC-72 droplets on heated smooth silicon surfaces and surfaces coated with nanofibers (CNF) of different length. Unexpectedly, we have found that the dynamic Leidenfrost temperature T_L , i.e., the transition temperature between the contact and film boiling regimes, is higher on the CNF surfaces than on smooth silicon surface. Increasing the fiber length from 3.5 μm to 7.5 μm causes T_L to increase significantly due to the small

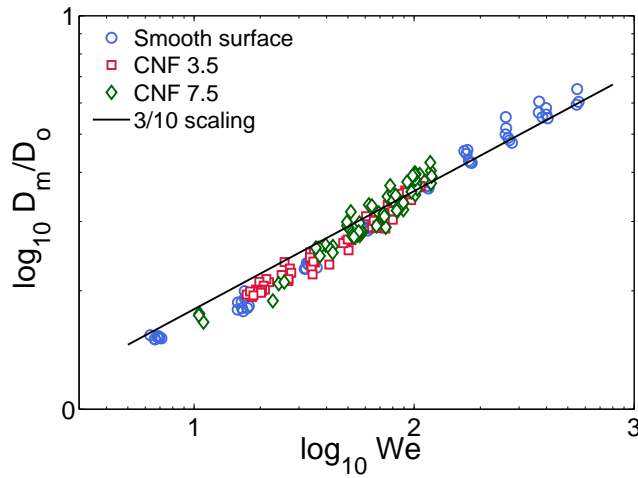


Figure 6: Spreading factor D_m/D_0 for impacting FC-72 droplets on three surfaces: smooth silicon, and silicon covered by a 3.5 μm - and a 7.5 μm -thick layer of carbon nanofibers. All the data points were obtained for impacts in the film boiling regime for which the impacting drop did not fragment in smaller droplets. The solid line represents the scaling relation $D_m/D_0 \sim We^{3/10}$ derived by taking the vapor flow as the major driving mechanism for the spreading of the liquid.¹⁶

time scale with which the nanofibers cool to the temperature of the vapor generated by the approaching liquid. Thus, the temperature of the fibers when contact with the liquid is established is much lower than their initial temperature. In other words, the temperature of the CNF surfaces has to be set higher than in the case of smooth silicon surfaces to bring the impact into film boiling regime. In contrast, the silicon microstructured surfaces studied in Ref.¹⁶ maintain their temperature during impact and T_L is lower, possibly because the liquid surface area which generates the vapor is larger due to the curvature caused by the micro-pillars.

In spite of the effect on T_L , we have found that, as long as the impact is in the film boiling regime, the spreading factor of the droplet does not depend on whether the surface is smooth or covered with carbon nanofibers, nor does it depend on the surface temperature. The spreading factor is consistent with the scaling law $D_m/D_0 \propto We^{3/10}$, which was derived based on the effect of vapor flow on the spreading dynamics.¹⁶

The increase in the dynamic Leidenfrost temper-

ature caused by nanofibers fabricated on silicon surfaces has a considerable implication for various applications that require high operating temperature because CNF surfaces can operate at higher T_L while still maintaining contact with the liquid.

Acknowledgement

This study was financially supported by the European Research Council ERC & FOM. We gratefully acknowledge Dr. Roald M. Tiggelaar and Stefan Schlautmann of MCS group for their assistance in the fabrication of Ni-Ta substrates for the CNF synthesis, M. Smithers (MESA+ Nanolab) for SEM imaging, B. Geerdink and Ruben Lubkemman for technical support.

References

- (1) Kim, J. *Int. J. Heat Fluid Flow* **2007**, 28, 753–767.
- (2) Agostini, B.; Fabbri, M.; Park, J. E.; Wojtan, L.; Thome, J. R.; Michel, B. *Heat Transfer Eng.* **2007**, 28, 258–281.
- (3) Ebadian, M. A.; Lin, C. X. *J. Heat Transfer* **2011**, 133, 110801.
- (4) Pautsch, A. G.; Shedd, T. A. *Int. J. Heat Mass Transfer* **2005**, 48, 3167–3175.
- (5) Visaria, M.; Mudawar, I. *IEEE Trans. Compon. Packag. Technol.* **2009**, 32, 784–793.
- (6) Arcoumanis, C.; Cutter, P.; Whitelaw, D. S. *Chem. Eng. Res. Des.* **1998**, 76, 124–132.
- (7) Panao, M. R. O.; Moreira, A. L. N. *Int. J. Thermal Sci.* **2009**, 48, 1853–1862.
- (8) Mascarenhas, N.; Mudawar, I. *Int. J. Heat Mass Transfer* **2012**, 55, 2953–2964.
- (9) Yoon, S. S.; Figueroa, V.; Brown, A. L.; Blanchat, T. K. *J. Fire Sci.* **2010**, 28, 109–139.
- (10) Chen, P.-P.; Wang, X.-S. *Int. J. Heat Mass Transfer* **2011**, 54, 4143–4147.

- (11) Moreira, A. L. N.; Moita, A. S.; Panão, M. R. *Prog. Energy Combust. Sci.* **2010**, *36*, 554–580.
- (12) Berberovic, E.; Roisman, I. V.; Jakirlic, S.; Tropea, C. *Int. J. Heat Fluid Flow* **2011**, *32*, 785–795.
- (13) Yarin, A. *Annu. Rev. Fluid Mech.* **2006**, *38*, 159–192.
- (14) Herbert, S.; Gambaryan-Roisman, T.; Stephan, P. *Colloids Surf. A* **2013**, *432*, 57–63.
- (15) Bernardin, J. D.; Stebbins, C. J.; Mudawar, I. *Int. J. Heat Mass Transfer* **1997**, *40*, 247–267.
- (16) Tran, T.; Staat, H. J. J.; Susarrey-Arce, A.; Foertsch, T. C.; van Houselt, A.; Gardeni-ers, J. G. E.; Prosperetti, A.; Lohse, D.; Sun, C. *Soft Matter* **2013**, *9*, 3272–3282.
- (17) Bernardin, J. D.; Mudawar, I. *J. Heat Transfer* **1999**, *121*, 894–903.
- (18) Wang, A. B.; Lin, C. H.; Chen, C. C. *Phys. Fluids* **2000**, *12*, 1622.
- (19) Bernardin, J. D.; Mudawar, I. *J. Heat Transfer* **2004**, *126*, 272–278.
- (20) Tran, T.; Staat, H. J. J.; Prosperetti, A.; Sun, C.; Lohse, D. *Phys. Rev. Lett.* **2012**, *108*, 036101.
- (21) Lee, J.; Kim, J.; Kiger, K. *Int. J. Heat Fluid Flow* **2001**, *22*, 188–223.
- (22) Weickgenannt, C. M.; Zhang, Y.; Sinha-Ray, S.; Roisman, I. V.; Gambaryan-Roisman, T.; Tropea, C.; Yarin, A. L. *Phys. Rev. E* **2011**, *84*, 036310.
- (23) Weickgenannt, C. M.; Zhang, Y.; Lembach, A. N.; Roisman, I. V.; Gambaryan-Roisman, T.; Yarin, A. L.; Tropea, C. *Phys. Rev. E* **2011**, *83*, 036305.
- (24) Chen, R. H.; Chiu, S. L.; Lin, T. H. *Appl. Therm. Eng.* **2007**, *27*, 2079–2085.
- (25) Chen, R.-H.; Chiu, S.-L.; Lin, T.-H. *Exp. Therm. Fluid Sci.* **2007**, *32*, 587–595.
- (26) Jun, S.; Sinha-Ray, S.; Yarin, A. L. *Int. J. Heat Mass Transfer* **2013**, *62*, 99–111.
- (27) Bitter, J. H. *J. Mater. Chem.* **2010**, *20*, 7312–7321.
- (28) Nair, H.; Tiggelaar, R. M.; Thakur, D. B.; Gardeni-ers, J. G. E.; van Houselt, A.; Lef-ferts, L. *Chem. Eng. J.* **2013**, *227*, 56–65.
- (29) Fujimoto, H.; Oku, Y.; Ogihara, T.; Takuda, H. *Int. J. Multiphase Flow* **2010**, *36*, 620–642.
- (30) Quéré, D. *Annu. Rev. Fluid Mech.* **2013**, *45*, 197–215.
- (31) Incropera, F. P.; DeWitt, D. P.; Bergman, T. L.; Lavine, A. S. *Fundamentals of Heat and Mass Transfer*, 7th ed.; Wiley, 2010.
- (32) Mandre, S.; Mani, M.; Brenner, M. P. *Phys. Rev. Lett.* **2009**, *102*, 134502.
- (33) Mayhew, E.; Prakash, V. *Carbon* **2013**, *62*, 493–500.